NeuroImage: Clinical 22 (2019) 101767

Contents lists available at ScienceDirect

NeuroImage: Clinical

journal homepage: www.elsevier.com/locate/ynicl

Quantification of white matter cellularity and damage in preclinical and early symptomatic Alzheimer's disease

Qing Wang[a,b,1], Yong Wang[a,b,c,d,e,*,1], Jingxia Liu[f], Courtney L. Sutphen[b,e,g], Carlos Cruchaga[e,h], Tyler Blazey[i], Brian A. Gordon[a,b], Yi Su[j], Charlie Chen[a], Joshua S. Shimony[a], Beau M. Ances[a,b,e,g], Nigel J. Cairns[b,k], Anne M. Fagan[b,e,g], John C. Morris[b,g], Tammie L.S. Benzinger[a,b,l]

[a] Mallinckrodt Institute of Radiology, Washington University School of Medicine, St. Louis, MO 63110, USA
[b] Knight Alzheimer's Disease Research Center, 4488 Forest Park, Suite 101, St. Louis, MO 63108, USA
[c] Department of Obstetrics and Gynecology, Washington University School of Medicine, St. Louis, MO 63110, USA
[d] Department of Biomedical Engineering, Washington University School of Engineering & Applied Science, St. Louis, MO 63015, USA
[e] Hope Center for Neurological Disorders, Washington University School of Medicine, St. Louis, MO 63110, USA
[f] Department of Surgery, Washington University School of Medicine, St. Louis, MO 63110, USA
[g] Department of Neurology, Washington University School of Medicine, St. Louis, MO 63110, USA
[h] Department of Psychiatry, Washington University School of Medicine, St. Louis, MO 63110, USA
[i] Division of Biology and Biomedical Sciences, Washington University School of Medicine, St. Louis, MO 63110, USA
[j] Banner Alzheimer's Institute, Phoenix, AZ 85006, USA
[k] Department of Pathology & Immunology, Washington University School of Medicine, St. Louis, MO 63110, USA
[l] Department of Neurosurgery, Washington University School of Medicine, St. Louis, MO 63110, USA

ARTICLE INFO

Keywords:
Inflammation
White matter damage
Diffusion basis spectrum imaging
Neuro-inflammation imaging
Cerebrospinal fluid
Preclinical Alzheimer disease
Early symptomatic Alzheimer disease
Magnetic resonance imaging

ABSTRACT

Interest in understanding the roles of white matter (WM) inflammation and damage in the pathophysiology of Alzheimer disease (AD) has been growing significantly in recent years. However, in vivo magnetic resonance imaging (MRI) techniques for imaging inflammation are still lacking. An advanced diffusion-based MRI method, neuro-inflammation imaging (NII), has been developed to clinically image and quantify WM inflammation and damage in AD. Here, we employed NII measures in conjunction with cerebrospinal fluid (CSF) biomarker classification (for β-amyloid (Aβ) and neurodegeneration) to evaluate 200 participants in an ongoing study of memory and aging. Elevated NII-derived cellular diffusivity was observed in both preclinical and early symptomatic phases of AD, while disruption of WM integrity, as detected by decreased fractional anisotropy (FA) and increased radial diffusivity (RD), was only observed in the symptomatic phase of AD. This may suggest that WM inflammation occurs earlier than WM damage following abnormal Aβ accumulation in AD. The negative correlation between NII-derived cellular diffusivity and CSF $A\beta_{42}$ level (a marker of amyloidosis) may indicate that WM inflammation is associated with increasing Aβ burden. NII-derived FA also negatively correlated with CSF t-tau level (a marker of neurodegeneration), suggesting that disruption of WM integrity is associated with increasing neurodegeneration. Our findings demonstrated the capability of NII to simultaneously image and quantify WM cellularity changes and damage in preclinical and early symptomatic AD. NII may serve as a clinically feasible imaging tool to study the individual and composite roles of WM inflammation and damage in AD.

Abbreviations: $A\beta_{42}$, CSF beta-amyloid; AD, Alzheimer disease; DBSI, diffusion basis spectrum imaging; FA, fractional anisotropy; CSF, cerebrospinal fluid; MRI, magnetic resonance imaging; NII, neuro-inflammation imaging; PET, positron emission tomography; TBSS, tract-based spatial statistics; t-tau, CSF total tau; WM, white matter; CNS, central nervous system; SNR, signal-to-noise ratio

* Corresponding author at: Department of Obstetrics and Gynecology, Washington University School of Medicine, 4901 Forest Park Ave. Suite 10201, COH, Saint Louis, MO 63108, USA.
E-mail address: wangyong@wustl.edu (Y. Wang).
[1] These two authors contributed equally to this paper.

https://doi.org/10.1016/j.nicl.2019.101767
Received 2 July 2018; Received in revised form 12 February 2019; Accepted 10 March 2019
Available online 13 March 2019
2213-1582/ © 2019 The Authors. Published by Elsevier Inc. This is an open access article under the CC BY-NC-ND license (http://creativecommons.org/licenses/BY-NC-ND/4.0/).

1. Introduction

Alzheimer disease (AD) leads to impaired memory and cognition culminating in dementia, loss of independence, and a heavy toll on patients and their families. A large body of evidence has supported the "amyloid hypothesis" that dysregulation of Aβ metabolism and the associated aggregation of Aβ into amyloid plaque leads to a pathophysiological process that results in synaptic dysfunction and neuronal death. Thus, numerous therapies specifically targeting Aβ have been tested in the past two decades (Blennow et al., 2010). However, > 100 candidate treatment compounds have failed to meet their clinical endpoints, leading to increasing interest in other possible AD-related pathophysiological mechanisms, such as accumulation of intracellular tau (Brier et al., 2016; Fagan et al., 2011; Gordon et al., 2016; Johnson et al., 2016), and more recently, inflammation (Heneka et al., 2015; Holtzman et al., 2012; Jarrott and Williams, 2016; Leyns et al., 2017; Suarez-Calvet et al., 2016).

Several lines of evidence point to the involvement of inflammation and white matter (WM) damage in early AD disease progression. First, cognitively normal individuals who chronically use non-steroidal anti-inflammatories have fewer activated microglia and lower risk of AD than non-users (Andersen et al., 1995; Broe et al., 2000; Cote et al., 2012). Fibrillar Aβ stimulates a classical proinflammatory response in microglia, which can be visualized in AD patients and may be present in preclinical AD (Bradshaw et al., 2013; Serrano-Pozo et al., 2013; Ulrich et al., 2018). A study of autosomal dominant AD suggested that astrocyte activation occurs in presymptomatic AD, indicating that inflammatory astrocytosis may contribute to early symptomatic AD pathology (Scholl et al., 2015). Moreover, disrupted WM may occur very early in preclinical AD (Heise et al., 2011; Molinuevo et al., 2014; Racine et al., 2014), promote phagocytosis of amyloid plaques (Smith et al., 2007a; Stokin et al., 2005), and modulate the relationship between the pathological and clinical manifestations of AD (Salat et al., 2009). Animal studies have recently demonstrated defective clearance of myelin debris, axonal dystrophy, and oligodendrocyte reduction in the triggering receptor expressed on myeloid cell 2 (TREM2)–deficient mice compared to wild-type mice (Cantoni et al., 2015; Poliani et al., 2015), suggesting microglial response to WM damage. These findings have led to a search for accurate and robust in vivo markers specific for inflammation and WM damage in AD.

A novel multi-parametric diffusion MRI analytic technique, diffusion basis spectrum imaging (DBSI), was developed to simultaneously detect and quantify inflammation and WM damage in the central nervous system. In particular, DBSI can discretely quantify intra- and extracellular water and allows for discrimination of vasogenic edema, increased cellularity, axonal injury/loss, and demyelination (Chiang et al., 2014; Wang et al., 2014; Wang et al., 2011; Wang et al., 2015). The DBSI biomarker for inflammation is the DBSI restricted water compartment, which is a surrogate for cellularity. DBSI cellularity increases have been associated with activated microglia and astrogliosis in multiple sclerosis (Chiang et al., 2014; Wang et al., 2014; Wang et al., 2011; Wang et al., 2015); therefore, it can be potentially employed as a marker for astrogliosis and microglial activation in AD. Moreover, DBSI can separate anisotropic diffusion markers (reflecting WM integrity) from isotropic diffusion markers, and are thus more specific and accurate in reflecting WM pathology than the standard model of diffusion tensor imaging (DTI) (Chiang et al., 2014; Wang et al., 2014; Wang et al., 2011; Wang et al., 2015). As initially conceived, DBSI employed diffusion MRI scans with 99 diffusion weightings. This protocol is not always available or optimal in clinical or clinical research settings. In the previous simulation and ex vivo study (Chiang et al., 2014), a compact 25-direction diffusion MRI scan provided sufficient accuracy in DBSI solutions. Here, we use the same 25-direction, multiple b-value diffusion MRI version of DBSI; We denote this clinical version of DBSI as neuro-inflammation imaging (NII). NII was used to study healthy cognitively normal controls, participants with preclinical (asymptomatic) AD, and participants with early symptomatic AD to better understand the role of WM inflammation and degeneration in the pathogenesis and progression of AD. The association between NII-derived indices and CSF biomarkers of AD pathology were examined to assess the relationship between WM inflammation, damage and AD Aβ and tau pathologies.

2. Materials and methods

2.1. Participants

Two hundred participants were enrolled in longitudinal clinical and biomarker studies of memory and aging at the Knight Alzheimer's disease Research Center at Washington University School of Medicine, St Louis, MO, USA (P50AG005681, P01AG026276, and P01AG003991). Details of recruitment and assessment have been published elsewhere (Berg et al., 1998). The Human Research Protection Office at Washington University approved all studies, and written informed consent was obtained from all participants. All individuals were evaluated by experienced clinicians using a semi-structured interview with a knowledgeable collateral source. Detailed neurological examinations of the participants were performed in accordance with the Uniform Data Set protocol of the National Alzheimer's Coordinating Center (Morris et al., 2006). A clinical diagnosis of symptomatic AD, where appropriate, was made in accordance with criteria developed by working groups from the National Institute on Aging and the Alzheimer's Association (Albert et al., 2011; McKhann et al., 2011). Dementia was staged according to the global Clinical Dementia Rating, CDR (Morris, 1993). The inclusion criteria required participants have CSF measures of amyloid ($A\beta_{42}$) and neurodegeneration (total tau [t-tau]) within two years of the MRI acquisition; Participants were classified as healthy controls ($n = 140$) if they were AD biomarker negative (CSF $A\beta_{42} \geq 459$ pg/ml and t-tau < 339 pg/ml) as defined previously (Vos et al., 2013) and cognitively normal defined as a CDR = 0 (Morris, 1993). Participants were classified as preclinical AD ($n = 34$) according to NIA-AA criteria (Sperling et al., 2011) if they had positive CSF $A\beta_{42}$ (CSF $A\beta_{42} < 459$ pg/ml) with normal cognition (CDR = 0). Early symptomatic AD participants ($n = 26$) had very mild dementia (CDR = 0.5), positive CSF $A\beta_{42}$ (CSF $A\beta_{42} < 459$ pg/ml) and these participants were diagnosed with dementia thought to be due to AD without other disease contribution, e.g., depression, cerebrovascular disease, etc. (McKhann et al., 2011). Other neuropsychological evaluations including the Mini-Mental Stage Exam (MMSE) and CDR sum of boxes were also provided.

2.2. Genotyping

DNA was extracted from peripheral blood samples by standard procedures. Apolipoprotein E genotyping was performed as previously described (Talbot et al., 1994). The presence of at least one apolipoprotein E ε4-allele was defined as *APOE* ε4 positive (*APOE* ε4 +).

2.3. CSF collection and analysis

CSF (20–30 ml) was collected within 24 months of the imaging session by routine lumbar puncture using a 22-gauge atraumatic Sprotte spinal needle (Pajunk Medical Systems, Norcross, GA, USA) after overnight fasting as previously described (Fagan et al., 2006). Samples were gently inverted to avoid possible gradient effects, briefly centrifuged at low speed, aliquoted (0.5 ml) into polypropylene tubes, and frozen at −84 °C. Samples were analyzed by ELISA for $A\beta_{42}$ and t-tau (INNOTEST; Fujirebio, formerly Innogenetics, Ghent, Belgium).

2.4. MRI acquisition

Diffusion MRI was collected on 3 T TIM Trio (Siemens, Erlangen, Germany) scanners with a 12-channel head coil equipped with parallel

imaging. The imaging resolution was $2 \times 2 \times 2\,mm^3$. Repetition time (TR) and echo time (TE) were 14,500 ms and 112 ms, respectively. The 25-direction diffusion-encoding scheme (24 diffusion sensitized +1 unsensitized [B_0] volumes) was implemented for data acquisition. The maximal b-value was 1400 s/mm^2. The full set of b-table is presented in Supplementary Table 3. Data were collected in two 6-min runs using a single-shot diffusion-weighted echo planar imaging sequence. Diffusion-weighted images were registered to T1-weighted (T1W) magnetization prepared rapid acquisition gradient echo (MPRAGE) and T2-weighted (T2W) fast spin echo (T2W-FSE) scans. The acquisition parameters for MPRAGE were the following: TR, 2400 ms; TE, 3.16 ms; inversion time, 1000 ms; imaging resolution, $1 \times 1 \times 1\,mm^3$. T2W-FSE was acquired with the following parameters: TR, 3200 ms; TE, 455 ms; imaging resolution, $1 \times 1 \times 1\,mm^3$.

2.4.1. Neuro-inflammation imaging

In neuro-inflammation imaging (NII), each of the potential pathological components, including inflammatory cell components, extracellular water/vasogenic edema, neuronal injury/loss, and demyelination, within each voxel is modeled by a dedicated diffusion tensor (Supplementary Fig. 1). The weighted sum of all sub-voxel pathological components describes the composition of pathological components as described in Eq. 1.

$$S_k = \sum_{i=1}^{N_{Aniso}} f_i e^{-|\overrightarrow{b_k}| \cdot \lambda_{\perp\_i}} e^{-|\overrightarrow{b_k}| \cdot (\lambda_{\parallel\_i} - \lambda_{\perp\_i}) \cdot \cos^2 \psi_{ik}} + \int_a^b f(D) e^{-|\overrightarrow{b_k}| D} dD \ (k = 1, 2, \ldots, K) \quad (1)$$

Specifically, NII models the entire diffusion-weighted MR signal as a linear combination of multiple anisotropic diffusion tensors (the first term in Eq. [1], representing crossing myelinated and unmyelinated axons of varied directions) and a spectrum of isotropic diffusion components (the second term, resulting from cells, sub-cellular structure, and edematous water). The quantities S_k and $|\overrightarrow{b_k}|$ are the signal and b-value of the k^{th} diffusion gradient, N_{Aniso} is the number of anisotropic tensors (fiber tracts), Ψ_{ik} is the angle between the k^{th} diffusion gradient and the principal direction of the i^{th} anisotropic tensor, $\lambda_{\parallel\_i}$ and $\lambda_{\perp\_i}$ are the axial and radial diffusivities of the i^{th} anisotropic tensor, f_i is the signal intensity fraction for the i^{th} anisotropic tensor, and a and b are the low and high diffusivity limits for the isotropic diffusion spectrum $f(D)$ (reflecting cellularity and edema). Similarly to DBSI (Wang et al., 2011; Wang et al., 2015), a two-step approach was employed to solve Eq. 1. In the first step, the number of anisotropic tensors (N_{Aniso}) and associated principal directions (Ψ_{ik}) were determined based on a diffusion bases decomposition approach (Ramirez-Manzanares et al., 2007). The second step was performed to determine $\lambda_{\parallel\_i}$ $\lambda_{\perp\_i}$ and f_i of each anisotropic tensor ($i = 1, 2 \ldots N_{Aniso}$) along with the isotropic diffusion spectrum $f(D)$ in Eq. (1) using a regularized least-squares cost function (Wang et al., 2011; Wang et al., 2015). Diffusion measurements with multiple directions and weightings are required for NII to provide a unique solution (Scherrer and Warfield, 2010; Scherrer and Warfield, 2012). Regularized nonnegative least-squares analysis incorporating a priori information of nonnegative signal intensities fraction (Scherrer and Warfield, 2012) and finite signal energy (Borgia et al., 1998; Borgia et al., 2000) are employed to prevent over-fitting to the noisy data while retaining the accuracy of the NII solution. By solving the NII model, the following indices were quantified: (1) cellular fraction (reflecting cell density); (2) cellular diffusivity (reflecting cell size); (3) FA (reflecting the WM integrity); (4) axial diffusivity (reflecting WM axonal injury); (5) radial diffusivity (reflecting WM demyelination); and (6) mean diffusivity (the average of axial and radial diffusivities). In particular, we define the isotropic diffusion components to represent restricted isotropic diffusion (associated with cellular components) by using a tentative threshold for isotropic diffusivity of 0.3 μm^2/ms, based on previous findings (Wang et al., 2011; Wang et al., 2015). Unlike DTI and other advanced diffusion MRI approaches, NII can detect and quantify the unique restricted isotropic signal signature reflecting inflammatory cells by excluding the confounding effects from anatomical complexity and WM degeneration.

2.5. Data processing and analysis

The 25 diffusion-weighted images acquired in one diffusion MRI sequence were motion-corrected by an iterative procedure. In order to correct for eddy current related geometric distortion between EPI diffusion images and 3D GRE/FSE anatomical images, we first registered the non-b0 diffusion images to b0 images with rigid body transformation. Then a 9-parametric affine transformation was employed to correct for stretch along the phase encode direction to better align the b0 image to the T2W image. Registration was completed by aligning the T2W images to the T1W images which were then aligned with the atlas image. The final resampling step output 24 volumes registered with the B_0 volume of the first acquired diffusion-weighted imaging dataset. The two runs were averaged together to obtain a better signal-to-noise ratio. All datasets were analyzed by a multi-tensor model analysis package developed in-house (Wang et al., 2011) in MATLAB (MathWorks) and maps of NII cellular fraction, cellular diffusivity, FA, axial, radial and mean diffusivities were generated.

The whole-brain, voxel-wise NII-derived indices were analyzed using Tract Based Spatial Statistics (TBSS) from the FSL (http://www.fmrib.ox.ac.uk/fsl) software package (Smith et al., 2007b; Smith and Nichols, 2009). NII FA images were slightly eroded, so the boundary image slices were excluded to remove possible outliers caused by poor diffusion tensor fitting at the edges. Participants' FA data were aligned into a common space using the nonlinear registration tool FNIRT (Jenkinson et al., 2002). A mean FA image was created and thinned to create a mean FA skeleton that represents the centers of all tracts common to the group. Each participant's aligned FA data, and other NII-derived indices, were projected onto this skeleton for statistical analyses. Nonparametric permutation tests were used for voxel-wise statistical analysis of the individual FA skeletons between the healthy controls, the preclinical AD and the early symptomatic AD cohorts. Voxel-wise associations between NII-derived indices and CSF markers of AD pathologies (CSF $A\beta_{42}$ and t-tau) were examined through TBSS. The significance threshold for group differences and associations with CSF biomarkers was set at $P < .05$, corrected for multiple comparisons by using a family-wise error correction across voxels by using the threshold-free cluster-enhancement option in Randomise 2.0 in FSL (Smith and Nichols, 2009). Identification of the abnormal WM tracts revealed by TBSS was based on the Johns Hopkins University (JHU) atlas (Hua et al., 2008; Mori and van Zijl, 2007; Wakana et al., 2004; Wakana et al., 2007). The statistical analyses performed by TBSS controlled for age, gender, and the presence of an *APOE* ε4 allele.

Continuous and categorical variables in characteristics across all the three groups were compared using the Kruskal-Wallis test and the Chi-square test, respectively. The least square means per group for each outcome were estimated after controlling for age, gender and *APOE* ε4 genotype. The partial correlation was also considered to measure the strength of a relationship between CSF measures and imaging metrics in WM tracts while controlling for the effects of other variables. All statistical tests were two-sided with $\alpha = 0.05$. SAS version 9.4 (Cary, NC) was used to perform all statistical analyses.

3. Results

3.1. Participant demographics

Demographic data are summarized in Table 1. Our cohort included 140 cognitively normal healthy control participants (CDR = 0.5, CSF $A\beta_{42}$-negative), 34 cognitively normal individuals with preclinical AD (CDR = 0.5, CSF $A\beta_{42}$-positive), and 26 participants with early symptomatic AD (CDR = 0.5, CSF $A\beta_{42}$-positive). On average, the early

Table 1
Characteristics of study participants.

Characteristics	Healthy controls	Preclinical AD	Early symptomatic AD	*P*-value
n	140	34	26	
Clinical dementia rating (CDR)	0	0	0.5	
Age, years	61.1 ± 8.1	62.6 ± 7.0	75.0 ± 5.7	< 0.001
Male sex	53 (37.9%)	11(32.4%)	16 (61.5%)	0.0468
APOE ε4 +	18 (12.9%)	26 (76.5%)	23 (88.5%)	< 0.001
MMSE	29.4 ± 0.9	29.3 ± 1.3	25.5 ± 2.7	< 0.001
CDR-sumbox	0.0 ± 0.1	0.0 ± 0.0	2.7 ± 1.0	< 0.001
CSF $A\beta_{42}$ (pg/ml)	786.1 ± 200.7	375.3 ± 76.1	325.1 ± 71.9	< 0.001
CSF t-tau (pg/ml)	206.9 ± 61.2	228.8 ± 101.8	507.4 ± 240.6	< 0.001

Data are presented as mean (SD) or number (%).
Healthy controls: participants with ≥ 459 pg/ml Aβ42 and ≤ 339 pg/ml total tau in the cerebrospinal fluid (CSF) and with normal cognition (CDR = 0).
Preclinical AD: participants with < 459 pg/ml Aβ42 in the CSF and with normal cognition (CDR = 0).
Early symptomatic AD: participants with < 459 pg/ml Aβ42 in the CSF and with very mild AD dementia (CDR = 0.5).
APOE ε4 +, positive for at least one apolipoprotein E ε4-allele.
MMSE: Mini-Mental State Exam.

symptomatic AD individuals were significantly older than the healthy controls and preclinical AD individuals, and the early symptomatic AD group included more male participants than the other two cohorts. Only 12.9% of the healthy controls carried at least one *APOE* ε4 allele, whereas 76.5% of the preclinical AD and 88.5% of the early symptomatic AD participants carried this allele. MMSE and CDR sum of box measures for early symptomatic AD were significantly higher than those in the healthy controls and preclinical AD group. The CSF level of $A\beta_{42}$ in the healthy controls was significantly higher than that in the preclinical and early symptomatic AD. The CSF level of t-tau was significantly elevated in the early symptomatic AD, while no difference was seen between the healthy controls and the preclinical AD participants.

3.2. NII cellular fraction in the preclinical and early symptomatic AD

No voxel-wise statistical differences of the NII cellular fraction (reflecting cell density) were found among the healthy controls, the preclinical, and the early symptomatic AD cohorts. As an example, the averaged NII cellular fraction in the region of genu of corpus callosum is 4.5% (± 1.1%) for the healthy controls, 4.5% (± 0.8%) for the preclinical AD and 4.4% (± 1.3%) for the early symptomatic AD.

3.3. NII cellular diffusivity in the preclinical and early symptomatic AD

Elevated NII cellular diffusivity (reflecting cell size) was observed in the preclinical AD cohort when compared to the healthy controls in the major WM tracts including corpus callosum, internal capsule, corona radiata and cingulum etc. (Fig. 1A). NII cellular diffusivity was also significantly increased in the early symptomatic AD cohort when compared to those in the preclinical AD in some major WM tracts (Fig. 1B). As an example, the significant voxels common to all participants in the genu of corpus callosum were extracted to demonstrate significantly increasing NII cellular diffusivity in the preclinical AD when compared to the healthy controls, and the further increasing of this index in the early symptomatic AD cohort ($P < .05$) (Fig. 1C). Similar findings were also found in other white matter tracks and summarized in Supplementary Table 1.

3.4. Relationship between NII biomarker of inflammation and CSF biomarker of amyloid plaque

NII cellular diffusivity was negatively correlated with CSF levels of $A\beta_{42}$ in major WM tracts (Fig. 2A and Supplementary Table 2) when analyzed across all groups. The mean NII cellular diffusivity from the cluster located in the genu of corpus callosum were extracted. As an estimate of effect size, the partial correlations were also examined between NII imaging markers and CSF $A\beta_{42}$. When controlling with age, gender and *APOE* ε4 genotype, the partial correlation with CSF $A\beta_{42}$ was $r_{partial} = -0.39$ ($P < .001$) for NII cellular diffusivity.

3.5. NII-derived FA, axial, radial and mean diffusivities in the preclinical and early symptomatic AD

A significant voxel-wise decrease of NII FA was found in the early symptomatic AD cohort when compared to the healthy controls and the preclinical AD cohorts in most of the WM tracts (Fig. 3A & B and Supplementary Table 1). The significant voxel-wise increase of NII radial diffusivity, which is a more accurate measure of the myelination than its DTI-derived counterpart (Wang et al., 2011; Wang et al., 2015), was also found in the early symptomatic AD cohort when compared to the healthy controls and the preclinical AD cohorts in most of the WM tracts (Fig. 3C & D and Supplementary Table 1). There were no differences of NII FA and radial diffusivity between the healthy controls and the preclinical AD cohorts. The significant voxels common to all participants in the genu of corpus callosum were extracted to demonstrate there were a significant decrease of NII-derived FA (Fig. 3E. (a) and a significant increase of NII radial diffusivity (Fig. 3E. (b) in the early symptomatic AD cohort when compared to the healthy controls and the preclinical AD cohorts ($P < .05$). No differences were found among the three cohorts for NII axial and mean diffusivities.

3.6. Relationship between NII-derived indices and CSF t-tau

A significant negative relationship was found between CSF levels of t-tau and NII FA in WM (Fig. 4A and Supplementary Table 2). No other NII-derived indices were associated with CSF levels of t-tau. The partial correlations as a measure of effect size were also examined between NII FA and CSF tau in those voxels that were significant in the splenium of corpus callosum. When controlling for age, gender and *APOE* ε4 genotype, the partial correlation with CSF t-tau was $r_{partial} = -0.33$ ($P < .001$) for NII FA.

4. Discussion

Immune cells, particularly microglia and astrocytes, have been reported to mediate the inflammatory response in AD and are considered a significant contributor to AD pathogenesis. Detecting and quantifying the early neuroinflammation manifested in AD as immune cell activation and infiltration could shed light on potential mechanisms underlying AD pathogenesis and progression. Based on the previous success of DBSI (Chiang et al., 2014; Wang et al., 2014; Wang et al., 2011;

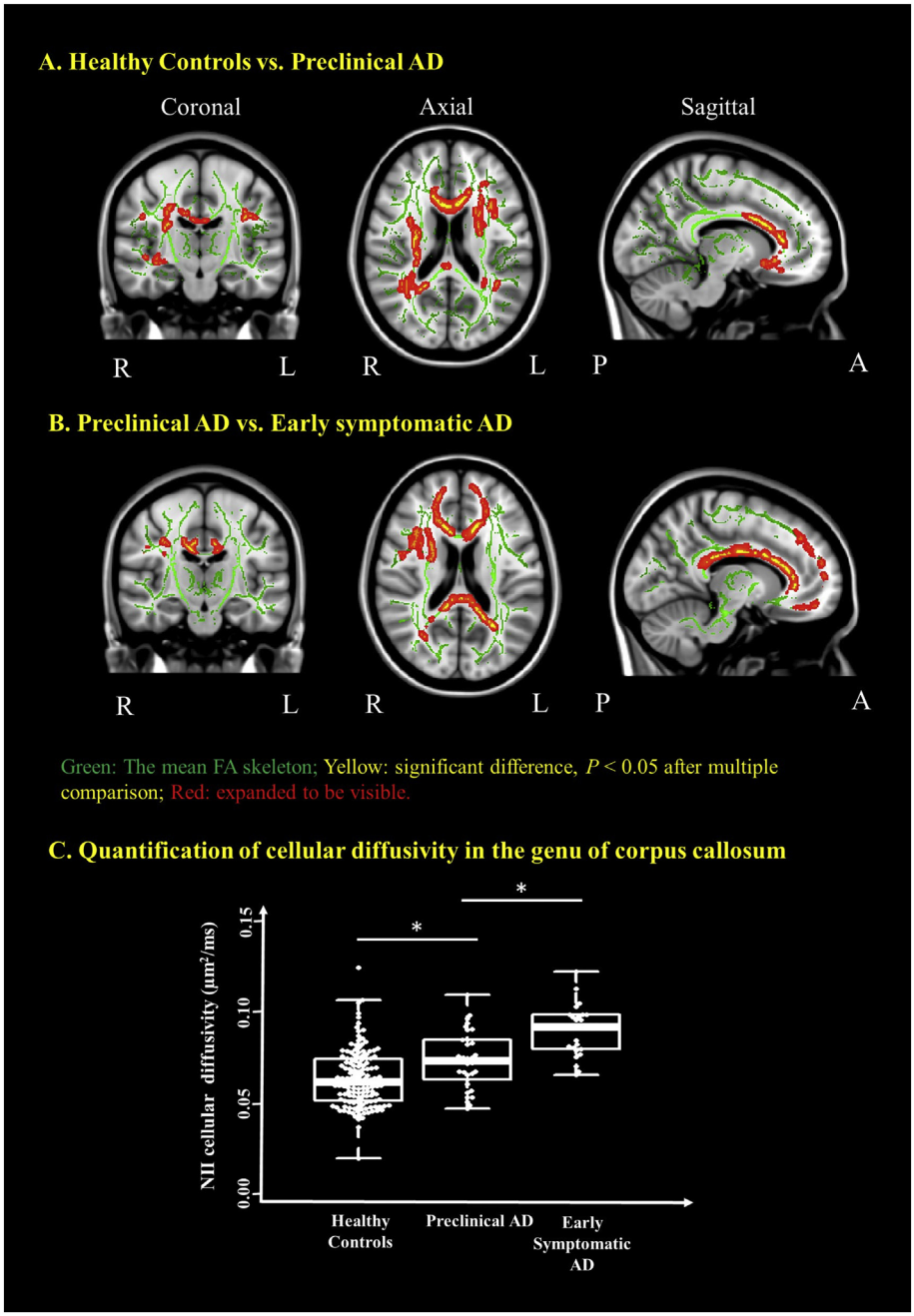

Fig. 1. Neuro-inflammation imaging (NII) detects increased cellular diffusivity in the preclinical AD and in the early symptomatic AD when compared to the healthy control participants. Coronal, axial and sagittal views show the voxels (red/yellow clusters, expanded to be visible) in which NII cellular diffusivity (reflecting cell size) significantly ($P < .05$) increased (1) in preclinical AD after multiple comparison when compared to the healthy controls cohort (A) and (2) in the early symptomatic AD cohort when compared to the preclinical AD cohorts (B). The mean FA skeleton (green) representing the centers of all WM tracts common to participants was overlaid on the Montreal Neurological Institute standard space brain T1-weighted image. (C) Boxplot demonstrates that the NII cellular diffusivity in the region of genu of corpus callosum is significantly increased in the preclinical AD and further significantly increased in the early symptomatic AD when compared to that in the healthy controls. Thick lines indicate means, boxes indicate 25th to 75th percentiles, and thin lines indicate 5th and 95th percentiles. The age, gender, and *APOE* e4 genotype were controlled for in computing the statistical significance of differences. L, left hemisphere; R, right hemisphere; P, posterior; A, anterior; *$P < .05$. (For interpretation of the references to color in this figure legend, the reader is referred to the web version of this article.)

Wang et al., 2015), NII was developed and implemented on clinical scanners to simultaneously detect and quantify WM cellularity change, which may reflect inflammation and WM damage, and their associations with CSF measures of AD pathologies in preclinical and early symptomatic AD.

Currently, three major types of biomarkers of inflammation in AD have been evaluated, but none have proved ideal. First, PET tracers such as [^{11}C]-(*R*)-PK11195, [^{11}C]-PBR28, [^{11}C]-DPA-713, [^{18}F]-DPA-714, [^{18}F]-FEPPA, which target the 18 kDa translocator protein (TSPO) (a marker for neuroinflammation), are used for imaging of microglia activation and inflammation in AD animal models and patients (Abourbeh et al., 2012; Chauveau et al., 2009; Hamelin et al., 2016b; Schuitemaker et al., 2013; Suridjan et al., 2015). Okello et al. found that activated microglia labeled by increased [^{11}C]-(*R*)-PK11195 binding was observed in prodromal participants with increased Pittsburgh compound B ([^{11}C]-PIB) retention for Aβ plaque load in brain (Okello et al., 2009). Another study found elevated microglial activation, as labeled by high [^{11}C]-(*R*)-PK11195 binding, in a group of AD subjects with high [^{11}C]-PIB retention (Edison et al., 2008). However, these PET approaches are limited by issues including binding tied to genetic polymorphisms (Owen et al., 2011; Owen et al., 2012), lackingspecificity of translocator protein binding for activated microglia (Kreisl et al., 2013; Lavisse et al., 2012) and variability of plasma protein binding (Turkheimer et al., 2015). Additionally, most of the current TSPO PET tracers are [^{11}C] based and can only be performed at academic centers in proximity to a research cyclotron facility (Fan et al., 2015; Varley et al., 2015). Elevated levels of CSF YKL40 (Craig-Schapiro et al., 2010) and other proteins have also been reported to be markers of inflammation (Alcolea et al., 2015; Heppner et al., 2015; Wilkins et al., 2015). Astroglial activation suggested by the elevated CSF levels of YKL40 has been observed in preclinical AD, mild cognitive impairment and early AD (Alcolea et al., 2015; Antonell et al., 2014; Craig-Schapiro et al., 2010; Olsson et al., 2013). CSF levels of YKL40 are promising in discriminating between cognitively normal individuals

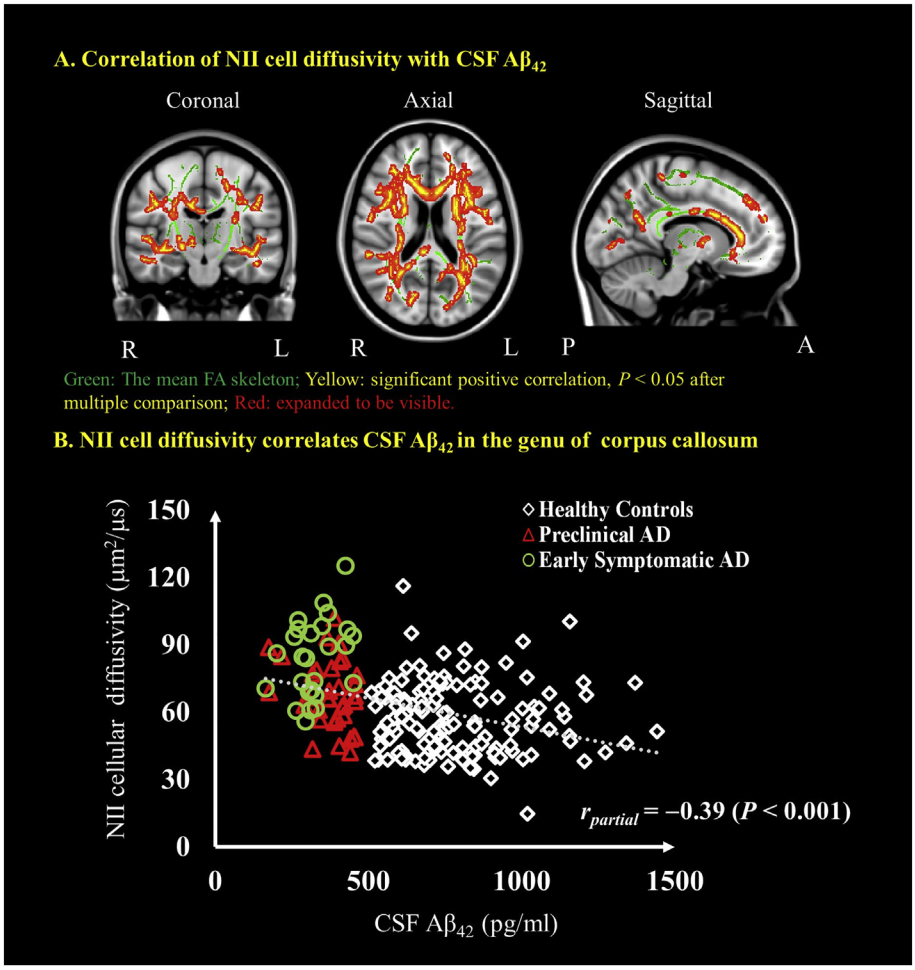

Fig. 2. Correlations between NII-derived indices and CSF $A\beta_{42}$. Coronal, axial and sagittal views show the voxel-wise significant ($P < .05$) (red/yellow clusters, expanded to be visible) correlations between NII cellular diffusivity and CSF $A\beta_{42}$ (A). The mean FA skeleton (green) representing the centers of all WM tracts common to all participants was overlaid on the Montreal Neurological Institute standard space brain T1-weighted image. Cluster-based thresholding corrected for multiple comparisons. (B) Scatter plot showing the association between NII cellular diffusivity and the CSF marker of β-amyloid in the genu of the corpus callosum. Diamond marker represents the healthy controls, red triangle represents the preclinical AD and the green circle represents the early symptomatic AD participants. The age, gender and *APOE* ε4 genotype were controlled for in computing the statistical significance of differences. L, left hemisphere; R, right hemisphere; P, posterior; A, anterior. (For interpretation of the references to color in this figure legend, the reader is referred to the web version of this article.)

and patients with mild cognitive impairment (MCI) and AD, and in predicting the progression of cognitively normal individuals to MCI (Kester et al., 2015). However, CSF analyses have limitations including potential assay drift (Schindler et al., 2018), inter-laboratory variability in measurements of certain markers (Mattsson et al., 2010; Mattsson et al., 2011; Mattsson et al., 2013), the invasiveness of a lumbar puncture and an inability to provide information about the anatomic location of pathology (Zetterberg, 2015). Given these limitations, as a non-invasive, non-radioactive imaging technique capable of quantifying cellular alterations which may reflect inflammation in the general population, NII holds a unique position to potentially advance our understanding of the role of inflammation in pre-symptomatic and early symptomatic AD.

In the present study, the lack of statistical difference of the NII cellular fraction among healthy controls, preclinical and early symptomatic AD suggests that there is no increase in inflammatory cell fraction (whether from proliferation or infiltration) in preclinical and early symptomatic AD. Microglia/astrocyte activation involves a rapid alteration of cellular metabolism and function, which can be accompanied by a graded spectrum of morphological changes that transform highly ramified microglia/astrocytes into amoeboid-phagocytic microglia/astrocytes with an increase in cell body size (Iaccarino et al., 2016; Soltys et al., 2001; Torres-Platas et al., 2014). A few diffusion MRI techniques have demonstrated their sensitivity to fiber or cell diameters by tracking the changes of water diffusion (Alexander et al., 2010; Barazany et al., 2009; Schachter et al., 2000; Stanisz et al., 1997). Increased cellular diffusivity which would be correspond with an increase in cell body size may serve as a potential marker for microglia/astrocyte activation in AD. In this study, NII derived cellular diffusivity was quantified in each group to reflect the extent of activated microglia/astrocytes. The observed increase of NII cellular diffusivity (Fig. 1) in the preclinical AD and early symptomatic AD group may suggest the microglia/astrocyte activation.

Emerging studies have demonstrated that microglial activation can promote Aβ clearance and play important role in neuroprotection during the early stage of AD (Gandy and Heppner, 2013; Solito and Sastre, 2012; Yang et al., 2011). The observed increase of NII cellular diffusivity (Fig. 1) and absence of WM damage according to NII-derived FA and radial diffusivity findings (Fig. 3) in the preclinical stage suggest the microglia/astrocyte activation may be the early pathological signature in AD. These results would be consistent with the neuroprotective role of early inflammation induced by Aβ. With progression of disease, chronic inflammation may stimulate pro-inflammatory cytokines and cause neuronal death (Czeh et al., 2011; Lucin and Wyss-Coray, 2009). NII findings in symptomatic AD may indicate the presence of chronic WM inflammation (Fig. 1) accompanied by wide spread WM damage, particularly myelin damage more than axonal injury (Fig. 3). These results are consistent with previous PET studies which found microglial activation in early preclinical AD to be protective (Hamelin et al., 2016a) and animals studies that have shown a detrimental role of chronic inflammation and neuronal loss in the later stage of AD (Leyns and Holtzman, 2017; Leyns et al., 2017; Wyss-Coray and Mucke, 2002).

Previous cross sectional DTI studies on sporadic AD and MCI patients reported widespread WM damages indicated by reduced FA and increased mean diffusivity (Agosta et al., 2011; Amlien and Fjell, 2014; Birdsill et al., 2014; Bosch et al., 2012; Kantarci et al., 2017; Madhavan et al., 2016; Sexton et al., 2011). Those WM regions include corpus

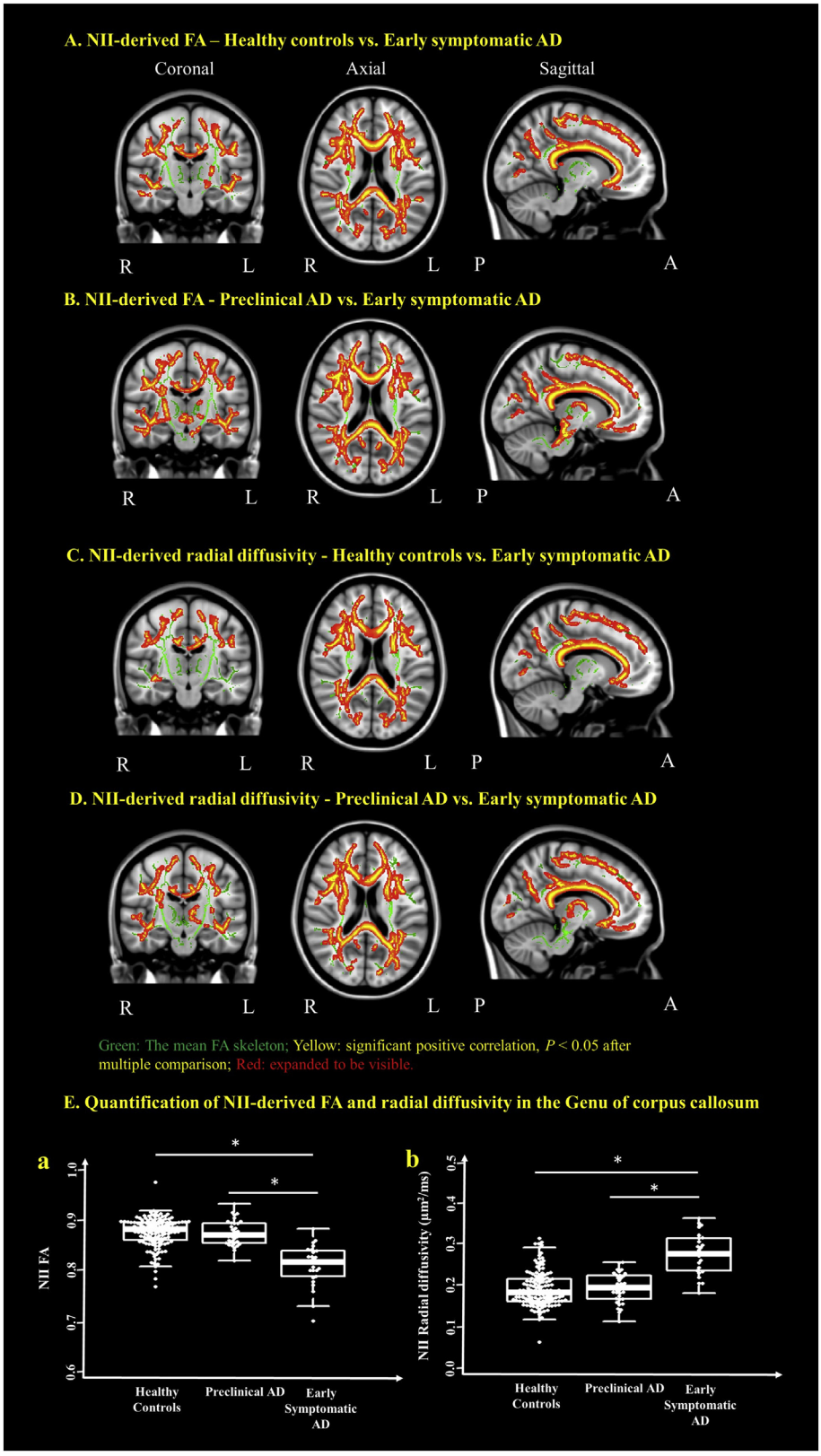

Fig. 3. NII detects decreased FA and increased radial diffusivity in the early symptomatic AD when compared to preclinical AD and healthy controls. Coronal, axial and sagittal views show the voxels (red/yellow clusters, expanded to be visible) in which (1) FA significantly ($P < .05$) decreased in early symptomatic AD after multiple comparison when compared to the healthy controls (A) and the preclinical AD (B) cohorts; (2) radial diffusivity significantly increased in the early symptomatic AD cohort when compared to the healthy controls (C) and the preclinical AD (D) cohorts. The mean FA skeleton (green) representing the centers of all WM tracts common to participants was overlaid on the Montreal Neurological Institute standard space brain T1-weighted image. (E) Boxplot demonstrates that, in the region of genu of corpus callosum, the FA (a) is significantly decreased and radial diffusivity (b) is significantly increased in the early symptomatic AD when compared to that in the preclinical AD and the healthy controls cohorts. Thick lines indicate means, boxes indicate 25th to 75th percentiles, and thin lines indicate 5th and 95th percentiles. The age, gender, and *APOE* ε4 genotype were controlled for in computing the statistical significance of differences. L, left hemisphere; R, right hemisphere; P, posterior; A, anterior; $*P < .05$. (For interpretation of the references to color in this figure legend, the reader is referred to the web version of this article.)

callosum, internal capsule, corona radiata, cingulum, fornix, superior longitudinal faciculus and superior fronto-occipital fasciculus, uncinated fasciculus etc., which largely overlap with the WM damage regions detected by reduced NII FA and increased NII radial diffusivity. WM microstructural changes have also been reported in aged adults without dementia using free water elimination DTI (Hoy et al., 2017). With more advanced modeling, NII detected increased cellular diffusivity, unchanged FA and radial diffusivity in the genu, body and splenium corpus callosum, internal capsule, corona radiata, posterior thalamic radiation, external capsule, fornix, etc. (Supplementary Table 1) in those with preclinical AD. Those findings may indicate WM inflammation occurs earlier than WM damage following abnormal

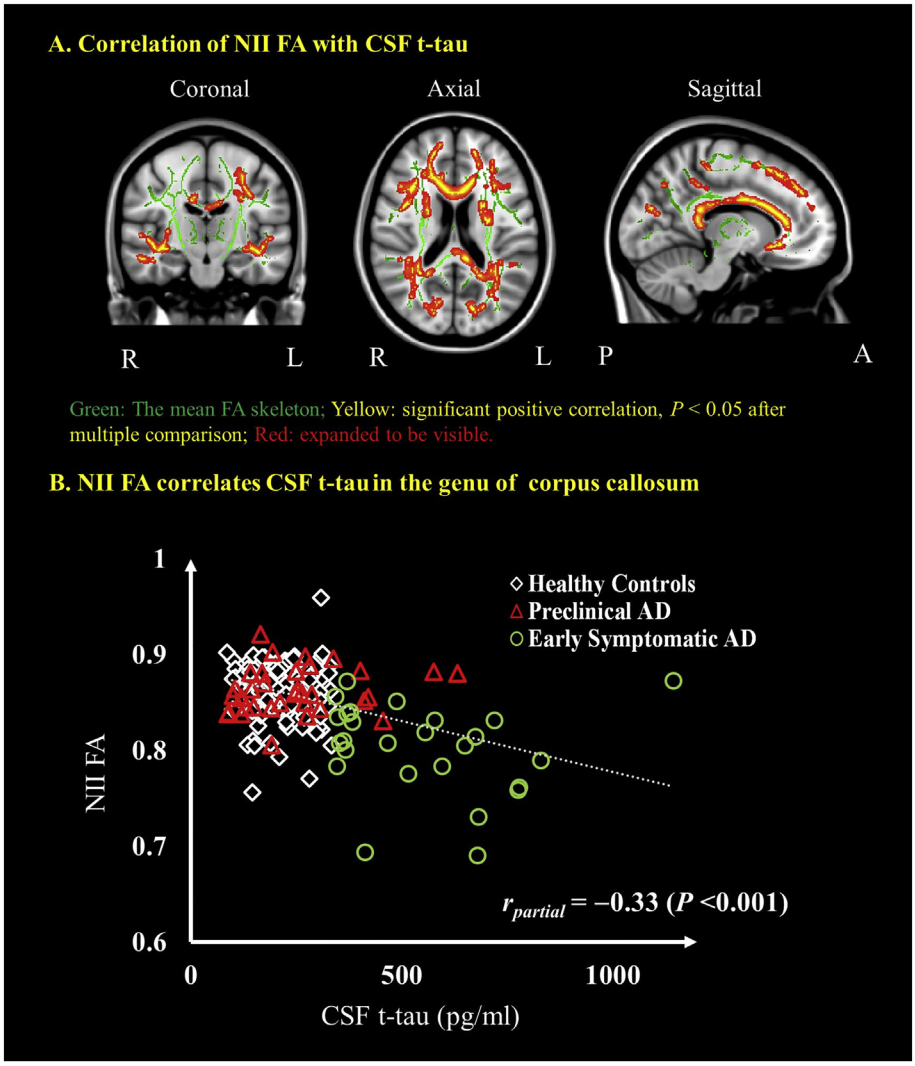

Fig. 4. Correlations between NII-derived FA and CSF tau. Coronal, axial and sagittal views show the voxel-wise significant ($P < .05$) (red/yellow clusters, expanded to be visible) correlations between NII FA and CSF t-tau (A) The mean FA skeleton (green) representing the centers of all WM tracts common to all participants was overlaid on the Montreal Neurological Institute standard space brain T1-weighted image. Cluster-based thresholding corrected for multiple comparisons. Scatter plots show the correlation between NII-derived indices and the CSF t-tau in the region of genu of corpus callosum (B). Diamond marker represents the healthy controls, red triangle represents the preclinical AD and the green circle represents the early symptomatic AD participants. The age, gender and *APOE* ε4 genotype were controlled for in computing the statistical significance of differences. L, left hemisphere; R, right hemisphere; P, posterior; A, anterior. (For interpretation of the references to color in this figure legend, the reader is referred to the web version of this article.)

amyloid accumulation in the preclinical AD period.

Abnormal amyloid deposition is considered an early AD pathology preceding tau accumulation (Bateman et al., 2012; Fagan et al., 2014). Fibrillar Aβ stimulates a classical proinflammatory response in microglia, which can be visualized in AD patients and may be present in preclinical AD (Bradshaw et al., 2013; Serrano-Pozo et al., 2013; Ulrich et al., 2018). Our finding of a significant correlation between NII WM inflammation measure (cellular diffusivity) and CSF $A\beta_{42}$ (Fig. 2A) is consistent with previous histological examination of AD brains as well as cell culture studies (Perlmutter et al., 1990), suggesting the WM involvement of the Aβ stimulated neuroinflammation. In contrast, CSF t-tau levels did not elevate in preclinical group and did not impact on the early WM inflammation detected by NII. Cerebral Aβ deposition and persistent activated microglia might both induce neuronal damage (Morales et al., 2014; von Bernhardi et al., 2010), which has been quantitatively measured by CSF t-tau. The observed association between CSF t-tau levels and NII WM damage measure in our cohort suggests the WM involvement of the neurodegeneration process in early symptomatic AD. The elevation of CSF $A\beta_{42}$ levels in preclinical group without NII-detected WM damage may suggest the delayed impact of amyloid deposition on WM damage. Although the biological mechanisms still remain unknown, the different associations between AD hallmark pathologies and NII WM measures may suggest the distinct impacts of amyloid deposition and neurofibrillary tangles on WM integrity.

Widespread WM damage such as demyelination was observed and associated with cognitive decline in individuals with symptomatic AD (Nir et al., 2013; O'Dwyer et al., 2011; Stebbins and Murphy, 2009). In this study, we found increased NII radial diffusivity and decreased NII FA in multiple white matter tracks (Supplementary Table 1) in early symptomatic AD, suggesting early involvement of demyelination and WM damage. Significant correlation between NII FA and CSF levels of t-tau (Fig. 4) suggests that WM abnormalities become more severe with increasing neurodegeneration.

The two tensor model (Pasternak et al., 2009) and other advanced diffusion MRI models (Collier et al., 2018; Edwards et al., 2017; White et al., 2013) have been previously proposed to eliminate the partial volume effect from free water, such as CSF, by including a free water compartment. In comparison to previous diffusion MRI methods, NII computes a spectrum of isotropic diffusion compartments to quantify not only free water, but also restricted, hindered water compartments, reflecting cellularity infiltration and edema, respectively, in CNS degenerative diseases (Chiang et al., 2014; Wang et al., 2011; Wang et al., 2015). In order to model the complex pathologies, NII employs a data-driven multiple tensor platform to analyze diffusion signals and adaptively determine the number and properties of diffusion compartments by solving an inverse problem.

Our previous studies have found that the accuracy and precision of DBSI computation depends on the SNR of diffusion MRI images (Chiang et al., 2014). From the Monte-Carlo simulation, no difference from the true values for the DBSI derived metrics was observed using 25- and 99-direction diffusion schemes. We found that a SNR larger than 30 should

be enough for DBSI computation. In our study, the averaged SNR in WM for each diffusion MRI acquisition is 45 on b0 images. With two repetitions of diffusion MRI acquisition, SNR can reach 63 on b0 images, which is sufficient for NII computation.

This study has several limitations. First, although NII has been validated for a different neurodegeneration disease, MS, there are no direct validations of NII's inflammation and WM damage indices in AD. We plan to validate NII by comparing with histopathology studies of AD autopsy brain, and other PET markers of inflammation such as DPA-714, PBR28 (Wang et al., 2009), PK11195(Shah et al., 1994). Another limitation is that new clinical neuropsychological tests such as Montreal cognitive assessment is not available in this study. Future studies will be needed to further clarify the level and types of cognitive impairment and its relationship with NII measures in the symptomatic group. Finally, longitudinal clinical studies will be needed to determine the relevance of NII indices in prediction of cognitive outcomes. Despite these limitations, our findings support NII's future applications to characterize AD progression. Moreover, NII can be readily deployed on most clinical MRI scanners and safely translated to clinical trials of larger patient populations.

5. Conclusion

AD is typically considered a disease of the gray matter. However, over the past several years, studies have reported abnormalities in white matter that are associated with disease progression. This study demonstrated that NII can simultaneously image and quantify WM cellularity changes and damage in preclinical and early symptomatic AD. With further validation and establishment, NII could be clinically translated to noninvasively investigate the roles of WM inflammation and damage in AD pathogenesis.

Acknowledgements

The authors thank all of the research volunteers for their contributions. The authors thank Dr. Sheng-Kwei Song, PhD, for his advice and Dr. Deborah J. Frank, PhD, for her help in editing the manuscript. This study was supported, in part, by grants from the National Institutes of Health (NIH) including the National Institutes on Aging (NIA) P01AG026276 (Antecedent Biomarkers of AD: the Adult Children Study, PI J. C. Morris); NIA P01AG003991 (Healthy Aging and Senile Dementia, PI J. C. Morris); NIA P50AG05681 (Alzheimer's disease Research Center, PI J. C. Morris); NIA 1R01AG054567-01A1(PIs T.L.S. Benzinger and Y. Wang,) and Washington University Institute of Clinical and Translational Sciences grant UL1 TR000448 from the National Center for Advancing Translational Sciences. This work used the services of the imaging facility informatics platform, supported by NIH grant 5P30NS048056 (PI D. S. Marcus). This work was also funded by a grant from the National Multiple Sclerosis Society RG5265 A1 (PI Y. Wang). Additional support was generously provided by the Charles and Joanne Knight Alzheimer's Research Initiative and by the Fred Simmons and Olga Mohan Fund and the Paula and Rodger Riney Fund. Support was also provided by NIH U54 HD087011 the Eunice Kennedy Shriver National Institute of Child Health & Human Development of the National Institutes of Health to the Intellectual and Developmental Disabilities Research Center at Washington University (PI J.S. Shimony).

Author contributions

Q.W., Y.W., T.L.S.B., J.S.S., B.M.A., Y. S., N.J.C., A.M.F., and J.C.M. designed the research; Q.W., Y.W., T.L.S.B., J.S.S., T.B., B.A.G., Y.S., C.L.S, E.M.H., N.J.C., A.M.F., and J.C.M. performed the research. Q.W., Y.W., T.B., Y.S., J.L., C.L.S, E.M.H. analyzed data, and Q.W., Y.W., T.L.S.B., B.A.G., Y.S., B.M.A., A.M.F., and J.C.M. wrote the paper.

Appendix A. Supplementary data

Supplementary data to this article can be found online at https://doi.org/10.1016/j.nicl.2019.101767.

References

Abourbeh, G., et al., 2012. Imaging microglial/macrophage activation in spinal cords of experimental autoimmune encephalomyelitis rats by positron emission tomography using the mitochondrial 18 kDa translocator protein radioligand [(1)(8)F]DPA-714. J. Neurosci. 32, 5728–5736.
Agosta, F., et al., 2011. White matter damage in Alzheimer disease and its relationship to gray matter atrophy. Radiology 258, 853–863.
Albert, M.S., et al., 2011. The diagnosis of mild cognitive impairment due to Alzheimer's disease: recommendations from the National Institute on Aging-Alzheimer's Association workgroups on diagnostic guidelines for Alzheimer's disease. Alzheimers Dement. 7, 270–279.
Alcolea, D., et al., 2015. Amyloid precursor protein metabolism and inflammation markers in preclinical Alzheimer disease. Neurology 85, 626–633.
Alexander, D.C., et al., 2010. Orientationally invariant indices of axon diameter and density from diffusion MRI. Neuroimage. 52, 1374–1389.
Amlien, I.K., Fjell, A.M., 2014. Diffusion tensor imaging of white matter degeneration in Alzheimer's disease and mild cognitive impairment. Neuroscience. 276, 206–215.
Andersen, K., et al., 1995. Do nonsteroidal anti-inflammatory drugs decrease the risk for Alzheimer's disease? The Rotterdam study. Neurology. 45, 1441–1445.
Antonell, A., et al., 2014. Cerebrospinal fluid level of YKL-40 protein in preclinical and prodromal Alzheimer's disease. J. Alzheimers Dis. 42, 901–908.
Barazany, D., Basser, P.J., Assaf, Y., 2009. In vivo measurement of axon diameter distribution in the corpus callosum of rat brain. Brain. 132, 1210–1220.
Bateman, R.J., et al., 2012. Clinical and biomarker changes in dominantly inherited Alzheimer's disease. N. Engl. J. Med. 367, 795–804.
Berg, L., et al., 1998. Clinicopathologic studies in cognitively healthy aging and Alzheimer's disease: relation of histologic markers to dementia severity, age, sex, and apolipoprotein E genotype. Arch. Neurol. 55, 326–335.
Birdsill, A.C., et al., 2014. Regional white matter hyperintensities: aging, Alzheimer's disease risk, and cognitive function. Neurobiol. Aging 35, 769–776.
Blennow, K., et al., 2010. Cerebrospinal fluid and plasma biomarkers in Alzheimer disease. Nat. Rev. Neurol. 6, 131–144.
Borgia, G.C., Brown, R.J., Fantazzini, P., 1998. Uniform-penalty inversion of multi-exponential decay data. J. Magn. Reson. 132, 65–77.
Borgia, G.C., Brown, R.J., Fantazzini, P., 2000. Uniform-penalty inversion of multi-exponential decay data. II. Data spacing, T(2) data, systemic data errors, and diagnostics. J. Magn. Reson. 147, 273–285.
Bosch, B., et al., 2012. Multiple DTI index analysis in normal aging, amnestic MCI and AD. Relationship with neuropsychological performance. Neurobiol Aging. 33, 61–74.
Bradshaw, E.M., et al., 2013. CD33 Alzheimer's disease locus: altered monocyte function and amyloid biology. Nat. Neurosci. 16, 848–850.
Brier, M.R., et al., 2016. Tau and A beta imaging, CSF measures, and cognition in Alzheimer's disease. Sci. Transl. Med. 8.
Broe, G.A., et al., 2000. Anti-inflammatory drugs protect against Alzheimer disease at low doses. Arch. Neurol. 57, 1586–1591.
Cantoni, C., et al., 2015. TREM2 regulates microglial cell activation in response to demyelination in vivo. Acta Neuropathol. 129, 429–447.
Chauveau, F., et al., 2009. Comparative evaluation of the translocator protein radioligands 11C-DPA-713, 18F-DPA-714, and 11C-PK11195 in a rat model of acute neuroinflammation. J. Nucl. Med. 50, 468–476.
Chiang, C.W., et al., 2014. Quantifying white matter tract diffusion parameters in the presence of increased extra-fiber cellularity and vasogenic edema. Neuroimage. 101, 310–319.
Collier, Q., et al., 2018. Diffusion kurtosis imaging with free water elimination: a bayesian estimation approach. Magn. Reson. Med. 80, 802–813.
Cote, S., et al., 2012. Nonsteroidal anti-inflammatory drug use and the risk of cognitive impairment and Alzheimer's disease. Alzheimers Dement. 8, 219–226.
Craig-Schapiro, R., et al., 2010. YKL-40: a novel prognostic fluid biomarker for preclinical Alzheimer's disease. Biol. Psychiatry 68, 903–912.
Czeh, M., Gressens, P., Kaindl, A.M., 2011. The yin and yang of microglia. Dev. Neurosci. 33, 199–209.
Edison, P., et al., 2008. Microglia, amyloid, and cognition in Alzheimer's disease: an [11C](R)PK11195-PET and [11C]PIB-PET study. Neurobiol. Dis. 32, 412–419.
Edwards, L.J., et al., 2017. NODDI-DTI: estimating neurite orientation and dispersion parameters from a diffusion tensor in healthy white matter. Front. Neurosci. 11, 720.
Fagan, A.M., et al., 2006. Inverse relation between in vivo amyloid imaging load and cerebrospinal fluid A beta(42) in humans. Ann. Neurol. 59, 512–519.
Fagan, A.M., et al., 2011. Comparison of analytical platforms for cerebrospinal fluid measures of beta-amyloid 1-42, total tau, and p-tau181 for identifying Alzheimer disease amyloid plaque pathology. Arch. Neurol. 68, 1137–1144.
Fagan, A.M., et al., 2014. Longitudinal change in CSF biomarkers in autosomal-dominant Alzheimer's disease. Sci. Transl. Med. 6, 226ra30.
Fan, Z., et al., 2015. Can studies of neuroinflammation in a TSPO genetic subgroup (HAB or MAB) be applied to the entire AD cohort? J. Nucl. Med. 56, 707–713.
Gandy, S., Heppner, F.L., 2013. Microglia as dynamic and essential components of the amyloid hypothesis. Neuron. 78, 575–577.
Gordon, B.A., et al., 2016. The relationship between cerebrospinal fluid markers of Alzheimer pathology and positron emission tomography tau imaging. Brain. 139,

2249–2260.
Hamelin, L., et al., 2016a. Early and protective microglial activation in Alzheimer's disease: a prospective study using 18F-DPA-714 PET imaging. Brain. 139, 1252–1264.
Hamelin, L., et al., 2016b. Early and protective microglial activation in Alzheimer's disease: a prospective study using F-18-DPA-714 PET imaging. Brain. 139, 1252–1264.
Heise, V., et al., 2011. The APOE varepsilon4 allele modulates brain white matter integrity in healthy adults. Mol. Psychiatry 16, 908–916.
Heneka, M.T., et al., 2015. Neuroinflammation in Alzheimer's disease. Lancet Neurol. 14, 388–405.
Heppner, F.L., Ransohoff, R.M., Becher, B., 2015. Immune attack: the role of inflammation in Alzheimer disease. Nat. Rev. Neurosci. 16, 358–372.
Holtzman, D.M., Mandelkow, E., Selkoe, D.J., 2012. Alzheimer disease in 2020. Cold Spring Harb. Perspect. Med. 2.
Hoy, A.R., et al., 2017. Microstructural white matter alterations in preclinical Alzheimer's disease detected using free water elimination diffusion tensor imaging. PLoS One 12, e0173982.
Hua, K., et al., 2008. Tract probability maps in stereotaxic spaces: analyses of white matter anatomy and tract-specific quantification. Neuroimage. 39, 336–347.
Iaccarino, H.F., et al., 2016. Gamma frequency entrainment attenuates amyloid load and modifies microglia. Nature. 540, 230–235.
Jarrott, B., Williams, S.J., 2016. Chronic brain inflammation: the neurochemical basis for drugs to reduce inflammation. Neurochem. Res. 41, 523–533.
Jenkinson, M., et al., 2002. Improved optimization for the robust and accurate linear registration and motion correction of brain images. Neuroimage. 17, 825–841.
Johnson, K.A., et al., 2016. Tau positron emission tomographic imaging in aging and early Alzheimer disease. Ann. Neurol. 79, 110–119.
Kantarci, K., et al., 2017. White-matter integrity on DTI and the pathologic staging of Alzheimer's disease. Neurobiol. Aging 56, 172–179.
Kester, M.I., et al., 2015. Cerebrospinal fluid VILIP-1 and YKL-40, candidate biomarkers to diagnose, predict and monitor Alzheimer's disease in a memory clinic cohort. Alzheimers Res. Ther. 7, 59.
Kreisl, W.C., et al., 2013. In vivo radioligand binding to translocator protein correlates with severity of Alzheimer's disease. Brain. 136, 2228–2238.
Lavisse, S., et al., 2012. Reactive astrocytes overexpress TSPO and are detected by TSPO positron emission tomography imaging. J. Neurosci. 32, 10809–10818.
Leyns, C.E.G., Holtzman, D.M., 2017. Glial contributions to neurodegeneration in tauopathies. Mol. Neurodegener. 12, 50.
Leyns, C.E.G., et al., 2017. TREM2 deficiency attenuates neuroinflammation and protects against neurodegeneration in a mouse model of tauopathy. Proc. Natl. Acad. Sci. U. S. A. 114, 11524–11529.
Lucin, K.M., Wyss-Coray, T., 2009. Immune activation in brain aging and neurodegeneration: too much or too little? Neuron. 64, 110–122.
Madhavan, A., et al., 2016. Characterizing white matter tract degeneration in syndromic variants of Alzheimer's disease: a diffusion tensor imaging study. J. Alzheimers Dis. 49, 633–643.
Mattsson, N., Blennow, K., Zetterberg, H., 2010. Inter-laboratory variation in cerebrospinal fluid biomarkers for Alzheimer's disease: united we stand, divided we fall. Clin. Chem. Lab. Med. 48, 603–607.
Mattsson, N., et al., 2011. Cerebrospinal fluid microglial markers in Alzheimer's disease: elevated chitotriosidase activity but lack of diagnostic utility. NeuroMolecular Med. 13, 151–159.
Mattsson, N., et al., 2013. CSF biomarker variability in the Alzheimer's Association quality control program. Alzheimers Dement. 9, 251–261.
McKhann, G.M., et al., 2011. The diagnosis of dementia due to Alzheimer's disease: recommendations from the National Institute on Aging-Alzheimer's Association workgroups on diagnostic guidelines for Alzheimer's disease. Alzheimers Dement. 7, 263–269.
Molinuevo, J.L., et al., 2014. White matter changes in preclinical Alzheimer's disease: a magnetic resonance imaging-diffusion tensor imaging study on cognitively normal older people with positive amyloid beta protein 42 levels. Neurobiol. Aging 35, 2671–2680.
Morales, I., et al., 2014. Neuroinflammation in the pathogenesis of Alzheimer's disease. A rational framework for the search of novel therapeutic approaches. Front. Cell. Neurosci. 8, 112.
Mori, S., van Zijl, P., 2007. Human white matter atlas. Am. J. Psychiatry 164, 1005.
Morris, J.C., 1993. The clinical dementia rating (CDR): current version and scoring rules. Neurology. 43, 2412–2414.
Morris, J.C., et al., 2006. The uniform data set (UDS): clinical and cognitive variables and descriptive data from Alzheimer disease centers. Alzheimer Dis. Assoc. Disord. 20, 210–216.
Nir, T.M., et al., 2013. Effectiveness of regional DTI measures in distinguishing Alzheimer's disease, MCI, and normal aging. NeuroImage Clin. 3, 180–195.
O'Dwyer, L., et al., 2011. Multiple indices of diffusion identifies white matter damage in mild cognitive impairment and Alzheimer's disease. PLoS One 6, e21745.
Okello, A., et al., 2009. Microglial activation and amyloid deposition in mild cognitive impairment: a PET study. Neurology. 72, 56–62.
Olsson, B., et al., 2013. Microglial markers are elevated in the prodromal phase of Alzheimer's disease and vascular dementia. J. Alzheimers Dis. 33, 45–53.
Owen, D.R., et al., 2011. Mixed-affinity binding in humans with 18-kDa translocator protein ligands. J. Nucl. Med. 52, 24–32.
Owen, D.R., et al., 2012. An 18-kDa translocator protein (TSPO) polymorphism explains differences in binding affinity of the PET radioligand PBR28. J. Cereb. Blood Flow Metab. 32, 1–5.
Pasternak, O., et al., 2009. Free water elimination and mapping from diffusion MRI. Magn. Reson. Med. 62, 717–730.
Perlmutter, L.S., Barron, E., Chui, H.C., 1990. Morphological association between microglia and senile plaque amyloid in Alzheimers-disease. Neurosci. Lett. 119, 32–36.
Poliani, P.L., et al., 2015. TREM2 sustains microglial expansion during aging and response to demyelination. J. Clin. Invest. 125, 2161–2170.
Racine, A.M., et al., 2014. Associations between white matter microstructure and amyloid burden in preclinical Alzheimer's disease: a multimodal imaging investigation. NeuroImage Clin. 4, 604–614.
Ramirez-Manzanares, A., et al., 2007. Diffusion basis functions decomposition for estimating white matter intravoxel fiber geometry. IEEE Trans. Med. Imaging 26, 1091–1102.
Salat, D.H., et al., 2009. Regional white matter volume differences in nondemented aging and Alzheimer's disease. Neuroimage. 44, 1247–1258.
Schachter, M., et al., 2000. Measurements of restricted diffusion using an oscillating gradient spin-echo sequence. J. Magn. Reson. 147, 232–237.
Scherrer, B., Warfield, S.K., 2010. Why multiple b-values are required for multi-tensor models. Evaluation with a constrained log-Euclidean model. In: Proceedings of the 2010 IEEE International Conference on Biomedical Imaging. ISBI 2010, pp. 1389–1392.
Scherrer, B., Warfield, S.K., 2012. Parametric representation of multiple white matter fascicles from cube and sphere diffusion MRI. PLoS One 7, e48232.
Schindler, S.E., et al., 2018. Upward drift in cerebrospinal fluid amyloid beta 42 assay values for more than 10 years. Alzheimers Dement. 14, 62–70.
Scholl, M., et al., 2015. Early astrocytosis in autosomal dominant Alzheimer's disease measured in vivo by multi-tracer positron emission tomography. Sci. Rep. 5, 16404.
Schuitemaker, A., et al., 2013. Microglial activation in Alzheimer's disease: an (R)-[(1)(1)C]PK11195 positron emission tomography study. Neurobiol. Aging 34, 128–136.
Serrano-Pozo, A., et al., 2013. Differential relationships of reactive astrocytes and microglia to fibrillar amyloid deposits in Alzheimer disease. J. Neuropathol. Exp. Neurol. 72, 462–471.
Sexton, C.E., et al., 2011. A meta-analysis of diffusion tensor imaging in mild cognitive impairment and Alzheimer's disease. Neurobiol. Aging 32 (2322), e5–18.
Shah, F., et al., 1994. Synthesis of the enantiomers of [N-methyl-11C]PK 11195 and comparison of their behaviours as radioligands for PK binding sites in rats. Nucl. Med. Biol. 21, 573–581.
Smith, S.M., Nichols, T.E., 2009. Threshold-free cluster enhancement: addressing problems of smoothing, threshold dependence and localisation in cluster inference. Neuroimage. 44, 83–98.
Smith, K.D., et al., 2007a. In vivo axonal transport rates decrease in a mouse model of Alzheimer's disease. Neuroimage. 35, 1401–1408.
Smith, S.M., et al., 2007b. Acquisition and voxelwise analysis of multi-subject diffusion data with tract-based spatial statistics. Nat. Protoc. 2, 499–503.
Solito, E., Sastre, M., 2012. Microglia function in Alzheimer's disease. Front. Pharmacol. 3.
Soltys, Z., et al., 2001. Morphology of reactive microglia in the injured cerebral cortex. Fractal analysis and complementary quantitative methods. J. Neurosci. Res. 63, 90–97.
Sperling, R.A., et al., 2011. Toward defining the preclinical stages of Alzheimer's disease: recommendations from the National Institute on Aging-Alzheimer's Association workgroups on diagnostic guidelines for Alzheimer's disease. Alzheimer's Dementia 7, 280–292 the journal of the Alzheimer's Association.
Stanisz, G.J., et al., 1997. An analytical model of restricted diffusion in bovine optic nerve. Magn. Reson. Med. 37, 103–111.
Stebbins, G.T., Murphy, C.M., 2009. Diffusion tensor imaging in Alzheimer's disease and mild cognitive impairment. Behav. Neurol. 21, 39–49.
Stokin, G.B., et al., 2005. Axonopathy and transport deficits early in the pathogenesis of Alzheimer's disease. Science. 307, 1282–1288.
Suarez-Calvet, M., et al., 2016. sTREM2 cerebrospinal fluid levels are a potential biomarker for microglia activity in early-stage Alzheimer's disease and associate with neuronal injury markers. EMBO Mol. Med. 8, 466–476.
Suridjan, I., et al., 2015. In-vivo imaging of grey and white matter neuroinflammation in Alzheimer's disease: a positron emission tomography study with a novel radioligand, [F-18]-FEPPA. Mol. Psychiatry 20, 1579–1587.
Talbot, C., et al., 1994. Protection against Alzheimer's disease with apoE epsilon 2. Lancet. 343, 1432–1433.
Torres-Platas, S.G., et al., 2014. Morphometric characterization of microglial phenotypes in human cerebral cortex. J. Neuroinflammation 11, 12.
Turkheimer, F.E., et al., 2015. The methodology of TSPO imaging with positron emission tomography. Biochem. Soc. Trans. 43, 586–592.
Ulrich, J.D., et al., 2018. ApoE facilitates the microglial response to amyloid plaque pathology. J. Exp. Med. 215, 1047–1058.
Varley, J., Brooks, D.J., Edison, P., 2015. Imaging neuroinflammation in Alzheimer's disease and other dementias: recent advances and future directions. Alzheimers Dement. 11, 1110–1120.
von Bernhardi, R., Tichauer, J.E., Eugenin, J., 2010. Aging-dependent changes of microglial cells and their relevance for neurodegenerative disorders. J. Neurochem. 112, 1099–1114.
Vos, S.J., et al., 2013. Preclinical Alzheimer's disease and its outcome: a longitudinal cohort study. Lancet Neurol. 12, 957–965.
Wakana, S., et al., 2004. Fiber tract-based atlas of human white matter anatomy. Radiology. 230, 77–87.
Wakana, S., et al., 2007. Reproducibility of quantitative tractography methods applied to cerebral white matter. Neuroimage. 36, 630–644.
Wang, M., et al., 2009. Fully automated synthesis and initial PET evaluation of [11C]PBR28. Bioorg. Med. Chem. Lett. 19, 5636–5639.
Wang, Y., et al., 2011. Quantification of increased cellularity during inflammatory demyelination. Brain. 134, 3590–3601.

Wang, X., et al., 2014. Diffusion basis spectrum imaging detects and distinguishes coexisting subclinical inflammation, demyelination and axonal injury in experimental autoimmune encephalomyelitis mice. NMR Biomed. 27, 843–852.
Wang, Y., et al., 2015. Differentiation and quantification of inflammation, demyelination and axon injury or loss in multiple sclerosis. Brain. 138, 1223–1238.
White, N.S., et al., 2013. Probing tissue microstructure with restriction spectrum imaging: histological and theoretical validation. Hum. Brain Mapp. 34, 327–346.
Wilkins, H.M., et al., 2015. Mitochondrial lysates induce inflammation and Alzheimer's disease-relevant changes in microglial and neuronal cells. J. Alzheimers Dis. 45, 305–318.
Wyss-Coray, T., Mucke, L., 2002. Inflammation in neurodegenerative disease–a double-edged sword. Neuron. 35, 419–432.
Yang, C.N., et al., 2011. Mechanism mediating oligomeric A beta clearance by naive primary microglia. Neurobiol. Dis. 42, 221–230.
Zetterberg, H., 2015. Cerebrospinal fluid biomarkers for Alzheimer's disease: current limitations and recent developments. Curr. Opin. Psychiatry 28, 402–409.